

# Inverted hysteresis and negative remanence in a homogeneous antiferromagnet

L. Opherden,<sup>1,2,\*</sup> T. Bilitewski,<sup>3</sup> J. Hornung,<sup>1,2</sup> T. Herrmannsdörfer,<sup>1</sup> A. Samartzis,<sup>4,5</sup>  
A. T. M. N. Islam,<sup>4</sup> V. K. Anand,<sup>4</sup> B. Lake,<sup>4,5</sup> R. Moessner,<sup>3</sup> and J. Wosnitza<sup>1,2</sup>

<sup>1</sup>Hochfeld-Magnettlabor Dresden (HLD-EMFL), Helmholtz-Zentrum Dresden-Rossendorf, 01328 Dresden, Germany

<sup>2</sup>Institut für Festkörper- und Materialphysik, TU Dresden, 01062 Dresden, Germany

<sup>3</sup>Max-Planck-Institut für Physik komplexer Systeme, 01187 Dresden, Germany

<sup>4</sup>Helmholtz-Zentrum Berlin für Materialien und Energie GmbH, Hahn-Meitner Platz 1, 14109 Berlin, Germany

<sup>5</sup>Institut für Festkörperphysik, Technische Universität Berlin, Hardenbergstraße 36, 10623 Berlin, Germany

(Dated: February 14, 2018)

Magnetic remanence – found in bar magnets or magnetic storage devices – is probably the oldest and most ubiquitous phenomenon underpinning technological applications of magnetism. It is a macroscopic non-equilibrium phenomenon: a remanent magnetisation appears when a magnetic field is applied to an initially unmagnetised ferromagnet, and then taken away. Here, we present an inverted magnetic hysteresis loop in the pyrochlore compound  $\text{Nd}_2\text{Hf}_2\text{O}_7$ : the remanent magnetisation points in a direction *opposite* to the applied field. This phenomenon is exquisitely tunable as a function of the protocol in field and temperature, and it is reproducible as in a quasi-equilibrium setting. We account for this phenomenon in considerable detail in terms of the properties of non-equilibrium population of domain walls which exhibit a magnetic moment between domains of an ordered antiferromagnetic state which itself has zero net magnetisation. Properties and (non-equilibrium) dynamics of topological defects play an important role in modern spintronics, and our study adds an instance where a uniform field couples selectively to domain walls rather than the bulk.

The ‘all-in–all-out’ state of pyrochlore magnets plays an important role in the study of topological magnets on account of its role in the genesis of condensed-matter axion electrodynamics [1]. Here, we study its response to an applied field in the insulating magnetic pyrochlore compound  $\text{Nd}_2\text{Hf}_2\text{O}_7$ .

We report the observation of a fully inverted magnetic hysteresis loop probed by the dynamic susceptibility resulting in a negative remanence in the low-field part of the all-in–all-out ordered phase [Fig. 2(a,b)]. Whereas several pyrochlore compounds adopt the all-in–all-out structure [2–7] and form domains [8–11],  $\text{Nd}_2\text{Hf}_2\text{O}_7$  is the first all-in–all-out antiferromagnet where such a negative remanent magnetisation has been observed. The underlying all-in–all-out order in  $\text{Nd}_2\text{Hf}_2\text{O}_7$  is established below  $T_N = 0.48$  K and is stable for external magnetic fields up to  $\mu_0 H_{dc} = 0.27$  T [Fig. 3 and Fig. S2].

$\text{Nd}_2\text{Hf}_2\text{O}_7$  belongs to the class of cubic pyrochlore oxides of the composition  $R_2T_2O_7$  where  $R$  is typically a trivalent rare-earth ion and  $T$  a tetravalent transition-metal ion. In these structures the  $R$  and the  $T$  ions both form a sublattice of corner-sharing tetrahedra [Fig. 1]. An asymmetrical arrangement of eight bivalent oxygen ions around each  $R$  ion leads to a strong crystal electric field (CEF) splitting of their  $J+1$  multiplet by several hundred Kelvin [12]. The resulting CEF ground state is a pseudo spin-half state with a strong local anisotropy and the spins are forced to point along the corner-to-center direction of each tetrahedron corresponding to the four equivalent local  $\langle 111 \rangle$  directions of the cubic lattice. In the all-in–all-out state all spins in a tetrahedron either point in or out resulting in two distinct realisations: a fourth of the spins are oriented either parallel (AIAO) or

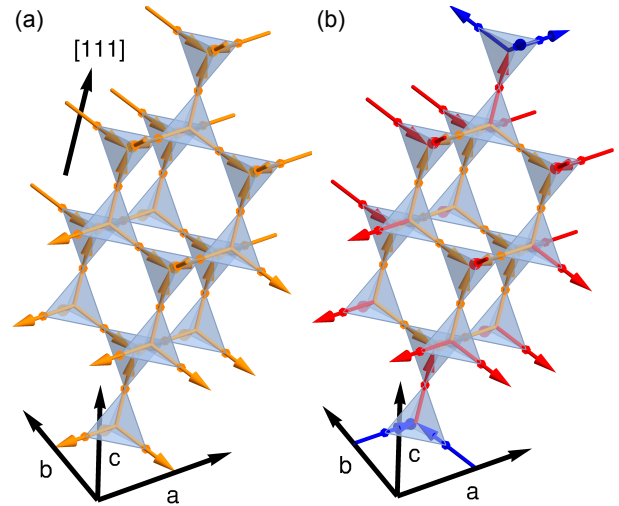


FIG. 1. Pyrochlore structure formed by a lattice of corner-sharing tetrahedra and all-in–all-out magnetic order. (a) All-in–all-out ordered state in the pyrochlore structure with a,b,c crystal axes and  $[111]$  direction indicated. All spins are oriented along their local  $\langle 111 \rangle$  direction pointing either into or out from the centre of their tetrahedra. Shown is the AIAO state, the AOAI state (not shown) is obtained by flipping all spins. (b) Spherical AIAO domain in AOAI background oriented along  $[111]$  resulting in a negative magnetisation. Blue (orange) spins belong to AOAI (AIAO) bulk tetrahedra, red spins are boundary spins of the AIAO domain.

antiparallel (AOAI) to the  $[111]$  axis. This allows for the formation of domains which we argue to be central to the experimental observations detailed next.

**Results:** The hysteresis behavior shows the following salient properties: There is (a) an inverted hysteresis loop

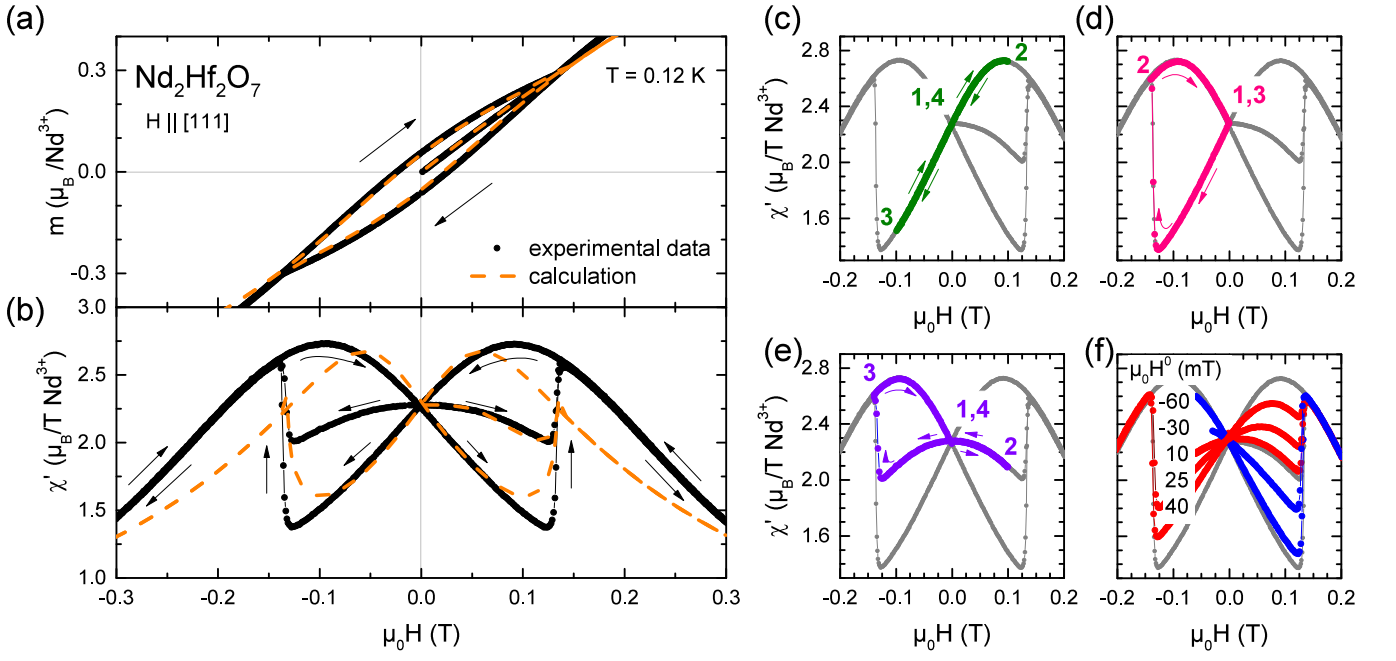


FIG. 2. Magnetic-field dependence of the dynamic susceptibility. (a) Experimental results (black line) and results from calculation (orange dashed line) of the magnetization (a) obtained by integrating the dynamic susceptibility (b), both for  $H \parallel [111]$  at a temperature of 0.12 K. For fields smaller than  $\pm 125$  mT ( $\pm H^*$ ) the susceptibility shows an inverted hysteresis. For higher fields a sharp transition to a polarised domain state is visible. (c) Staying below the critical field  $H^*$  the state is stable (d,e) The state can be changed by applying a high positive or negative field or by applying a heat pulse. (f) AC susceptibility for different applied fields  $H^0$  while cooling the sample below  $T_N$ .

with a large negative remanent magnetisation, (b) which is stable, reproducible and fully tunable by cooling the sample in a finite field, and (c) can be reset by applying a heat pulse above  $T_N$ ; finally, (d) it is highly anisotropic, only occurring for specific field directions.

The fully inverted hysteresis loop of  $\text{Nd}_2\text{Hf}_2\text{O}_7$  observed for  $H \parallel [111]$  [Fig. 2] covers a fixed area and appears only if the external magnetic field exceeds a certain temperature dependent value  $H^*(T)$  (up to 0.14 T at 0.12 K for  $H \parallel [111]$ ) where the susceptibility shows a sharp and pronounced jump [Fig. 2(b)].

In contrast, for fields oriented along the [001] direction we find no hysteresis [Fig. S2(b)]. At the same temperature  $H^*$  is significantly smaller than the critical field  $H_c$  at which the transition occurs for  $H \parallel [001]$  [Fig. S2(c)]. Further, it strongly depends on temperature for  $T \leq T_N$  [Fig. S3]. For temperatures higher than  $T_N$ , no hysteresis is observed.

We find a large coercivity, about 24 mT at a temperature of 0.12 K, to be compared to recent findings in ferromagnetic thin films which show a reversed hysteresis with a coercive field of only about 2 mT [13]. Also the remanence is unusually large at  $0.06 \mu_B/\text{Nd}^{3+}$ , 100 times larger than (the conventional 'non-inverted' hysteresis) in  $\text{Cd}_2\text{Os}_2\text{O}_7$  (up to  $6 \cdot 10^{-5} \mu_B/\text{Os}$ ) [11].

Next, we demonstrate that the sample adopts distinct stable states depending on the field/temperature history.

We start by considering the stability of the observed hysteresis curves to magnetic field changes. In Fig. 2(c,e) we show that when staying below  $H^*$  the magnetization is free of hysteresis and the state is perfectly stable. The susceptibility follows a unique perfectly reproducible trajectory when sweeping the magnetic field back and forth staying below  $H^*$ , both when in the polarised state [Fig. 2(c), green data points] as well as in the unpolarised state [Fig. 2(e), violet data].

Moreover, one can reliably switch between the different states of the system. In Fig. 2(d,e) we show such a protocol. Starting in the positive polarised or unpolarised state sweeping the field below  $-H^*$  switches the system to the negative polarised state in which the susceptibility follows a distinct stable trajectory. Then applying a thermal cycle above the critical temperature after switching off the field allows to return the sample to the unpolarised state.

Additionally, the observed hysteresis in the susceptibility may be continuously and fully tuned. By cooling the sample below  $T_N$  in a finite magnetic field  $|H^0| < |H^*|$ , we prepare a family of distinct stable states with associated susceptibility curves [Fig. 2(f)]. The observed trajectories continuously interpolate between the maximally polarised conditions. These states are again perfectly stable to changes in the magnetic field below the critical field with a unique trajectory defined by the initially

prepared state. This is in stark contrast to the known behavior of ferromagnetic materials where a field change or temperature variation within the ordered state leads to domain wall orientation, hence, a reduced hysteresis loop and different trajectories of  $m(H, T)$ .

Finally, we demonstrate that the AIAO ordered state of  $\text{Nd}_2\text{Hf}_2\text{O}_7$  splits into two distinct phases as seen in the AC susceptibility for external magnetic fields applied along [111] [Fig. 3] as well as [110] [Fig. S5]. At low fields and temperatures the system can adopt different states whereas at high fields a unique state appears.

For each field, the sample was cooled under an overcritical positive field (+), an overcritical negative field (-) and in zero field (0). At low temperatures the susceptibility of these states differs: the negatively polarised state showing a lower susceptibility than the positively polarised state and the unpolarised (zero field cooled) state being intermediate the polarised states.

For a sufficiently strong field we find a new phase setting in at larger temperatures where the susceptibility for the differently prepared states coincides before diverging at lower temperatures. The entrance into this unique state is accompanied by a sharp change of  $\chi'$  for the negatively and non-polarised states and the susceptibility only depends weakly on temperature within this phase. The temperature range where this state exists increases at increasing external field (blue shaded areas in Figs. 3 and S5). At an even higher temperature,  $\chi'(T)$  exhibits a peak (kink for higher fields) and the antiferromagnetic order is broken.

We construct the field-temperature phase diagram for  $H||[111]$  [Fig. 3(b)] by the temperature of the kink as well as by the endpoints of the hysteresis in the temperature and field dependence of the AC susceptibility [Fig. 3 and Fig. S3]. Whereas the kink represents the phase boundary to the all-in-all-out ordered state, the latter criteria separates the mixed domain state from the polarised domain state. In the Supplementary the corresponding phase diagrams for different field directions are provided.

*Discussion:* We interpret these results as originating from domains of the two possible realisations of the all-in-all-out order. At strong fields only the fully polarised domain state exists, whereas within the hysteretic part of the all-in-all-out state, the sample can contain any mixture of AIAO and AOAI domains. Preparing the sample in a finite field allows for tuning the ratio of AIAO to AOAI domains up to the fully polarised single domain state. The results then suggest that within each phase these domain configurations are stable to changes in temperature and magnetic field.

We propose an explanation of the anisotropic and inverted hysteresis and the negative remanent magnetization via the preferential formation of oppositely (to the magnetic field) polarised domain walls present within a non-magnetic bulk background phase. This explains (a)

the negative remanence, (b) the tunability of the hysteresis via cooling in a finite field, (c) the resetting of the sample state via a heat pulse and (d) the anisotropy.

We model the system via a free energy for a mixture of two bulk phases with different energies given by

$$f = x [E_{\text{AIAO}}(H) - E_{\text{AOAI}}(H)] + x(1-x) [E_{\text{DW}} - m_{\text{DW}}H] + T [x \ln(x) + (1-x) \ln(1-x)], \quad (1)$$

with the volume fraction  $x$  of the AIAO bulk phase, the corresponding bulk energies  $E_{\text{AIAO/AOAI}}$ , a contribution of the domain walls proportional to the surface between phases  $x(1-x)$  with associated cost  $E_{\text{DW}}$  due to broken bonds and magnetisation  $m_{\text{DW}}$ , and the mixing entropy between phases proportional to the temperature  $T$ .

For the comparison with the experimental hysteresis curves in Fig. 2(a,b) we use the energy and magnetisation of the bulk phases obtained from a classical treatment of the microscopic hamiltonian which reproduces the magnetisation behavior observed for magnetic fields oriented along [100] (see Supplementary). We emphasise that we do not fit parameters to the hysteric data, but rather use the parameters obtained from the non-hysteric magnetisation curve observed for a different field direction and obtain good agreement with the hysteric experimental data.

This model is based on the following key observations: The all-in-all-out state can be realized by two configurations, related to each other by flipping all spins on their Ising axis [Fig. 1]. Within the all-in-all-out order one fourth of the spins is parallel (AIAO configuration) or antiparallel (AOAI configuration) to the [111] direction. An effective canting of the spins out of their local Ising-anisotropy axis, as a result of the dipolar-octupolar nature of the  $\text{Nd}^{3+}$  ions, can lead to a gain of Zeeman energy which differs between these two configurations depending on the field direction [10]. In particular, for  $H||[111]$  the AIAO and AOAI states are split in energy. Thus, we model the system as a mixture of two bulk phases with an energy difference dependent on the applied magnetic field. We note that at zero field these bulk phases carry no magnetisation and are degenerate.

In contrast, for a field applied parallel to the [001] direction, the projection of the field onto the four  $\langle 111 \rangle$  directions is equal. Therefore, the field does not distinguish between the AIAO/AOAI states, the distribution of domains does not change when applying a field and, thus, the susceptibility is free of hysteresis.

At finite temperature both phases will be present to maximise the entropy which we model by including a mixing entropy in the free energy. Domain walls between the phases cost an energy  $E_{\text{DW}}$  due to the broken bonds at the boundary [Fig. 1(b)].

To explain the negative remanence we note that domain walls carry a magnetisation  $m_{\text{DW}}$ ; and that this magnetisation preferentially opposes the applied field.

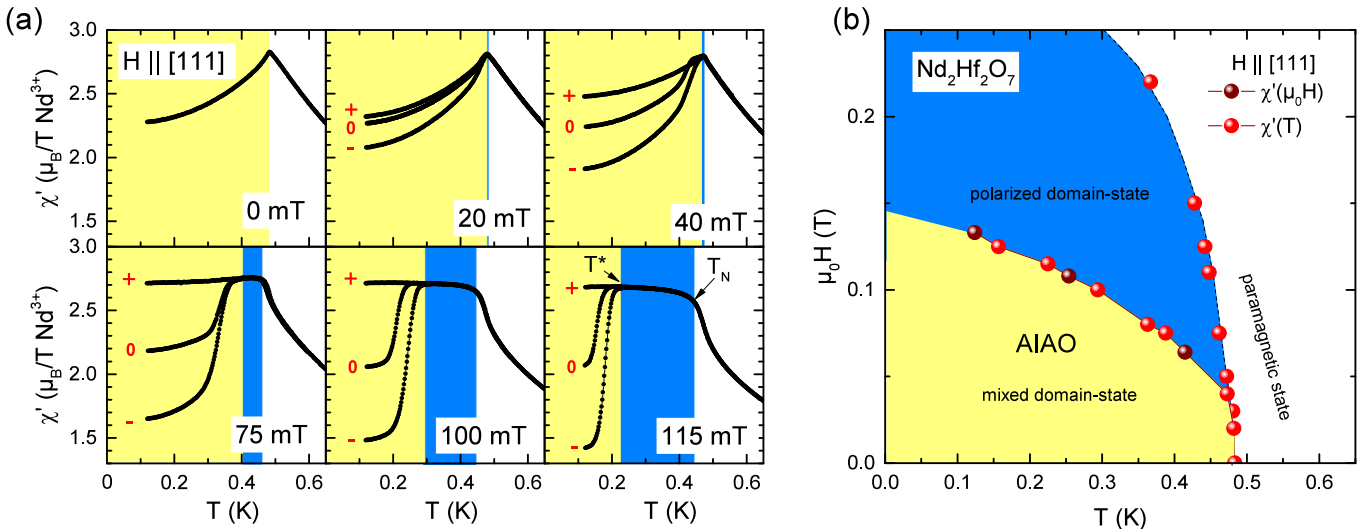


FIG. 3. (a) Temperature dependence of the dynamic susceptibility of  $\text{Nd}_2\text{Hf}_2\text{O}_7$  for magnetic DC fields applied along  $H \parallel [111]$ . The sample was prepared to be either in the positive polarised state (+), the negative polarised state (-) or the unpolarised state (0). The blue shaded area denotes the respective temperature range of the single domain state. (b) Phase diagram for  $\text{Nd}_2\text{Hf}_2\text{O}_7$  for  $H \parallel [111]$ . The phase boundary of the all-in-all-out order was determined by the kinks/peaks of  $\chi'(T)$  (red spheres). The border between the mixed domain phase and the polarised domain phase was constructed by taking the temperature at each field (red spheres) below which the AC susceptibility starts to differ when polarizing in negative compared to positive external fields  $|H| > H_c$  and the field strength of the end points of the hysteresis in the dynamic susceptibility (brown spheres). The thin black dashed line is a guide to the eye.

This happens because walls between AIAO and AOAI domains with a negative magnetisation are kinematically favoured as they have a lower energy barrier than walls with a positive magnetisation (see Supplementary). In consequence, once domains have formed at low temperature and finite field, the sample retains a negative remanent magnetization after removing the field: in zero field, both AIAO and AOAI domains have zero magnetisation, so that only that of the domain walls remains. We find that spherical domains carry a magnetization along one of the four equivalent  $\langle 111 \rangle$  directions [Fig. 1(b) and Supplementary].

Naturally, the magnetization of a random collection of domain walls vanishes. Thus, applying a heat pulse  $T > T_N$  to the sample allows a relaxation of the domains in which all symmetry equivalent domains are created equally, and the magnetization vanishes again.

By contrast, when preparing the sample in a partially polarised state by cooling down in a finite field, both AIAO and AOAI domains are present with a ratio determined by the field strength and tunable from fully positive to fully negatively polarised. The hysteresis thus follows the weighted average of the fully positively and fully negatively polarised sample states.

**Conclusions:** Our findings constitute, to the best of our knowledge, the first observation of an inverted hysteresis/negative remanence in a bulk antiferromagnet. The mechanism – a nonequilibrium population of negatively polarised domain walls – appears entirely novel. It invites

more detailed investigations, in particular with regard to the nucleation process leading to the disappearance of the phenomenon, and the spatial distribution of the domain walls themselves.

By contrast, previous instances of negative remanence were essentially ferri-magnetic in nature, in that they relied on the non-cancellation of moments of inequivalent ferromagnetic subsystems, either in form of thin films [13] or different ionic species [14].

Not only is our hysteresis loop highly reproducible and stable to magnetic field and temperature changes, but also exquisitely tunable. We demonstrate precise control of the system's response via the preparation of a continuous family of distinct non-equilibrium states.

Thus,  $\text{Nd}_2\text{Hf}_2\text{O}_7$  provides a non-equilibrium landscape controllable via small magnetic fields or temperature pulses. Controlled tunability of magnetic structures underpins the field of spintronics, and currently the search for novel types of magnetic structures and their manipulation is a central theme there. The preferential coupling in  $\text{Nd}_2\text{Hf}_2\text{O}_7$  of a weak field to domain walls provides an unusual handle on this unconventional magnet, while the antiferromagnetic domains themselves do not interact with each other via a bulk magnetisation. It is further promising that  $\text{Nd}_2\text{Hf}_2\text{O}_7$  may be prepared as epitaxially grown thin films of a few nanometer thickness [15]. Each of these items is desirable for technological applications underlining the potential for inclusion in submicron devices.

VI-521) and DFG through SFB 1143. We also acknowledge support by HLD at HZDR, member of the European Magnetic Field Laboratory (EMFL).

\* [l.opherden@hzdr.de](mailto:l.opherden@hzdr.de)

- [1] X. Wan, A. M. Turner, A. Vishwanath, and S. Y. Savrasov, *Phys. Rev. B* **83**, 205101 (2011).
- [2] E. Lhotel, S. Petit, S. Guitteny, O. Florea, M. Ciomaga Hatnean, C. Colin, E. Ressouche, M. Lees, and G. Balakrishnan, *Phys. Rev. Lett.* **115**, 197202 (2015).
- [3] J. Xu, V. K. Anand, A. K. Bera, M. Frontzek, D. L. Abernathy, N. Casati, K. Siemensmeyer, and B. Lake, *Phys. Rev. B* **92**, 224430 (2015).
- [4] A. Bertin, P. Dalmas de Réotier, B. Fåk, C. Marin, A. Yaouanc, A. Forget, D. Sheptyakov, B. Frick, C. Ritter, A. Amato, C. Baines, and P. J. C. King, *Phys. Rev. B* **92**, 144423 (2015).
- [5] Z. Tian, Y. Kohama, T. Tomita, H. Ishizuka, T. H. Hsieh, J. J. Ishikawa, K. Kindo, L. Balents, and S. Nakatsuji, *Nat Phys* **12**, 134 (2016).
- [6] J. J. Ishikawa, E. C. T. O’Farrell, and S. Nakatsuji, *Phys. Rev. B* **85**, 245109 (2012).
- [7] J. Yamaura, K. Ohgushi, H. Ohsumi, T. Hasegawa, I. Yamauchi, K. Sugimoto, S. Takeshita, A. Tokuda, M. Takata, M. Udagawa, M. Takigawa, H. Harima, T. Arima, and Z. Hiroi, *Phys. Rev. Lett.* **108**, 247205 (2012).
- [8] E. Y. Ma, Y.-T. Cui, K. Ueda, S. Tang, K. Chen, N. Tamura, P. M. Wu, J. Fujioka, Y. Tokura, and Z.-X. Shen, *Science* **350**, 538 (2015).
- [9] S. Tardif, S. Takeshita, H. Ohsumi, J.-i. Yamaura, D. Okuyama, Z. Hiroi, M. Takata, and T.-h. Arima, *Phys. Rev. Lett.* **114**, 147205 (2015).
- [10] L. Opherden, J. Hornung, T. Herrmannsdörfer, J. Xu, A. T. M. N. Islam, B. Lake, and J. Wosnitzer, *Phys. Rev. B* **95**, 184418 (2017).
- [11] H. T. Hirose, J.-i. Yamaura, and Z. Hiroi, *Sci. Rep.* **7**, 42440 (2017).
- [12] J. S. Gardner, M. J. P. Gingras, and J. E. Greedan, *Rev. Mod. Phys.* **82**, 53 (2010).
- [13] T. Maity, D. Kepaptsoglou, M. Schmidt, Q. Ramasse, and S. Roy, *Phys. Rev. B* **95**, 100401 (2017).
- [14] S.-I. Ohkoshi, T. Hozumi, and K. Hashimoto, *Phys. Rev. B* **64**, 132404 (2001).
- [15] F. Wei, H. Tu, and J. Du, *J. Phys. D: Appl. Phys.* **42**, 185301 (2009).
- [16] V. K. Anand, D. L. Abernathy, D. T. Adroja, A. D. Hillier, P. K. Biswas, and B. Lake, *Phys. Rev. B* **95**, 224420 (2017).
- [17] V. K. Anand, A. K. Bera, J. Xu, T. Herrmannsdörfer, C. Ritter, and B. Lake, *Phys. Rev. B* **92**, 184418 (2015).
- [18] Y.-P. Huang, G. Chen, and M. Hermele, *Phys. Rev. Lett.* **112**, 167203 (2014).
- [19] O. Benton, *Phys. Rev. B* **94**, 104430 (2016).
- [20] S. Petit, E. Lhotel, B. Canals, M. Ciomaga Hatnean, J. Ollivier, H. Mutka, E. Ressouche, A. R. Wildes, M. R. Lees, and G. Balakrishnan, *Nat Phys* **12**, 746 (2016).

### Acknowledgement

We acknowledge the Helmholtz Gemeinschaft for funding via the Helmholtz Virtual Institute (Project No. VH-

## SUPPLEMENTARY MATERIAL

### Experimental protocol

$\text{Nd}_2\text{Hf}_2\text{O}_7$  single crystalline samples were investigated by means of dynamic (AC) susceptibility using a pair of compensated coils with frequencies between 11 Hz and 11 kHz and field amplitudes,  $H_{\text{ac}}$ , between 1.8 and  $9.6 \mu\text{T}$ , and static (DC) magnetization at a field amplitude  $H_{\text{dc}}$  of 0.1 T using a commercial vibrating sample magnetometer. The AC-field direction was aligned parallel to the DC field. If not stated differently, the AC susceptibility was measured at  $f = 1111 \text{ Hz}$ . The single crystals were grown by the floating-zone technique using a high-temperature optical furnace.

### Influence of the AC frequency

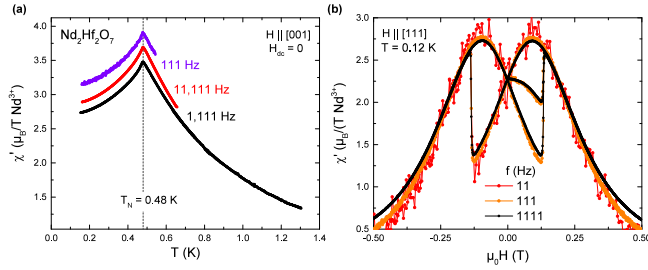


FIG. S1. Temperature (a) and magnetic field (b) dependence of the dynamic susceptibility without an external DC magnetic field for different frequencies of the AC magnetic field.

The influence of the frequency on the dynamic susceptibility for  $\text{Nd}_2\text{Hf}_2\text{O}_7$  was investigated by measuring the temperature dependence of  $\chi_{\text{ac}}$  for zero DC magnetic field and  $H_{\text{ac}} \parallel [001]$  [Fig. S1 (a)] as well as the field dependence for an external field along  $[111]$  at 0.12 K [Fig. S1 (b)].

In both cases the measured dynamic susceptibility does not depend on the used AC frequency over four orders of magnitude. Therefore we conclude that even at the highest measured frequency the spin system can still respond fully to the applied AC field and, thus, the dynamic susceptibility behaves in this frequency range as the static susceptibility  $\chi_{\text{dc}}$ . In consequence, the magnetization of  $\text{Nd}_2\text{Hf}_2\text{O}_7$  can be obtained by integrating the dynamic susceptibility

$$M \sim \int \chi_{\text{ac}} dH. \quad (\text{S1})$$

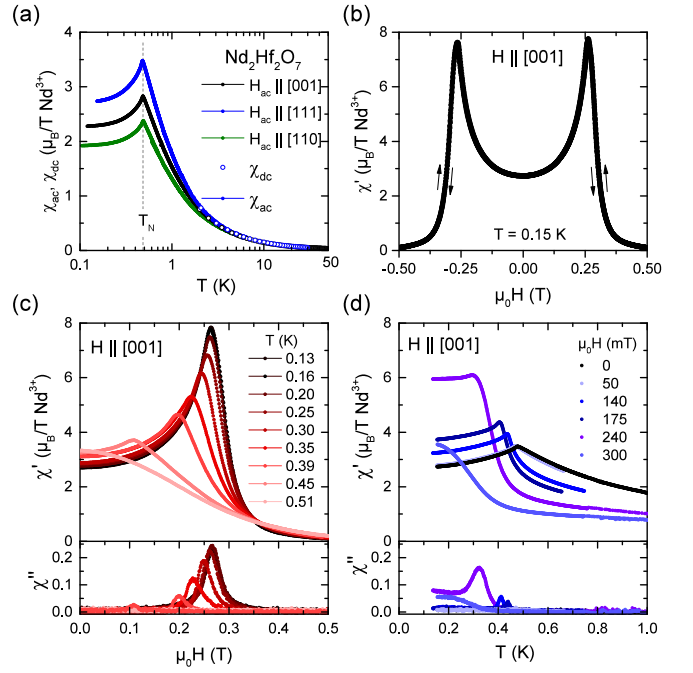


FIG. S2. Dynamic susceptibility of  $\text{Nd}_2\text{Hf}_2\text{O}_7$ . (a)  $\chi'_{\text{ac}}$  without an external magnetic field and  $\chi_{\text{dc}} = M/H$ . (b) Field dependence of  $\chi'$  for  $H \parallel [001]$  at a temperature of 0.15 K for a full hysteresis cycle. (c) Field dependence of  $\chi'$  and  $\chi''$  for  $H \parallel [001]$  for various temperature. (d) Temperature dependence of  $\chi'$  and  $\chi''$  for  $H \parallel [001]$  for various applied magnetic fields.

### Results for $H \parallel [001]$

The dynamic susceptibility of  $\text{Nd}_2\text{Hf}_2\text{O}_7$  in zero DC field follows a Curie-Weiss law above  $T_N$  and coincides with the static susceptibility ( $\chi_{\text{dc}} = M/H$ ).

At a temperature of  $T_N = 0.48 \text{ K}$  a cusp is visible [Fig. S2(a)]. This is a characteristic feature of the phase transition to the antiferromagnetically ordered all-in-all-out state [2, 10] as recently confirmed for  $\text{Nd}_2\text{Hf}_2\text{O}_7$  by neutron scattering and  $\mu\text{SR}$  experiments [16, 17]. (The ordering temperature was determined to be slightly higher in polycrystalline samples.)

The phase transition can also be seen in the field dependence of the AC susceptibility for an external magnetic field along  $[001]$  where  $\chi'$  shows a pronounced maximum and no sign of hysteresis [Fig. S2(b)]. The maximum in  $\chi'$  is accompanied by a peak in  $\chi''$ , centred at the same field  $H_c$ .

The intensities of both peaks are reduced if the temperature is increased towards  $T_N$  and  $H_c$  is lowered [Fig. S2(c)]. Above  $T_N$ , the susceptibility shows no maximum.

From this data the phase boundary of the all-in-all-out phase for  $H \parallel [001]$  was determined [black dots in Fig. S7(a)]. Further points of the phase boundary were obtained by measuring the temperature depen-

dence in presence of an external DC field [Fig. S2(d)] and analysing the peak temperature of  $\chi''$  [grey dots in Fig. S7(a)].

### Behavior of the [111]-hysteresis for different temperatures

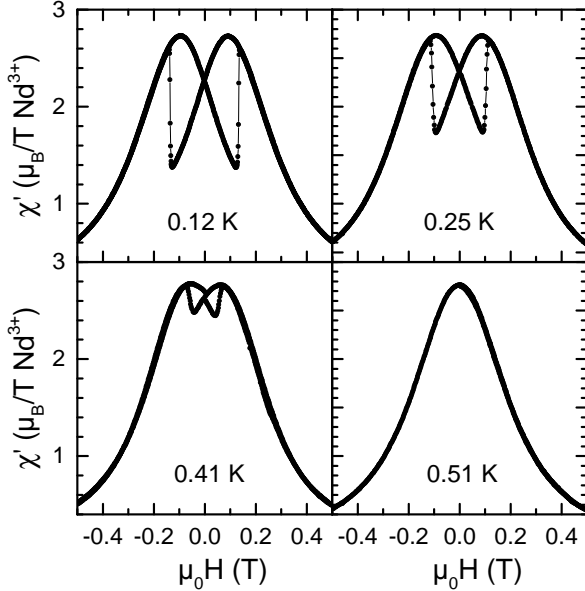


FIG. S3. Magnetic field dependence of the dynamic susceptibility for different temperatures and  $H||[111]$ .

The critical field below which a hysteresis is observed in the dynamic susceptibility of  $\text{Nd}_2\text{Hf}_2\text{O}_7$  for  $H||[111]$  is reduced at larger temperatures (Fig. S3). Whereas the difference between the positively and negatively polarised state within the multiple domain phase at a constant temperature remains nearly unchanged, the field width of the hysteresis is decreasing.

Furthermore, the width of the transition also increases with increasing temperature. If the temperature exceeds the Néel temperature  $T_N$  of 0.48 K the hysteresis vanishes completely.

### Hysteresis for $H || [110]$

For an applied field along [110] an inverted hysteresis loop is observed as well [Fig. S4].

Whereas the hysteresis extends over a larger field range (Fig. S4) the difference between the positive and negative polarised states is smaller than for a field along [111] (see Fig. 3(a) and Fig. S5).

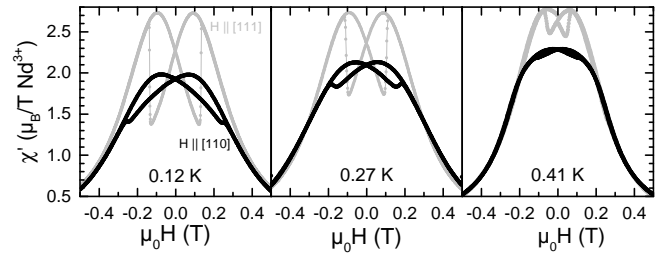


FIG. S4. Comparison of the AC susceptibility hysteresis for an applied field parallel to [110] (black) and [111] (grey) for different temperatures.

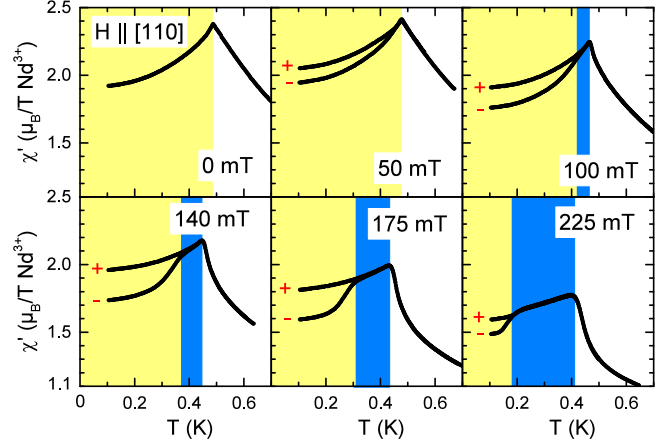


FIG. S5. Temperature dependence of the dynamic susceptibility for different preparation fields in the orientation  $H||[110]$ . The sample was prepared to be either in the positively polarised state (+) or the negatively polarised state (-). The blue shaded area denotes the respective temperature range of the single domain state.

### Comparison of all main field directions

The strong anisotropic behavior of  $\text{Nd}_2\text{Hf}_2\text{O}_7$  can be most clearly seen in the direct comparison of all three main directions (Fig S6).

While for  $H||[001]$  the phase transition has the most drastic effect on the dynamic susceptibility, no hysteresis can be observed [panels (a) and (b)].

In contrast both for  $H||[111]$  [panels (c) and (d)] and for  $H||[110]$  [panels (e) and (f)] an inverted hysteresis loop is found. In comparison the hysteresis loop for  $H||[111]$  extends over a smaller field range, but shows a larger response than for  $H||[110]$ .

In Fig S7 we compare the resulting phase diagrams for the three main field directions.

As described above we obtain the phase-boundary of the hysteresis-free all-in-all-out order for  $H||[001]$  [panel (a)] from the temperature and field dependence of the dynamic susceptibility shown in Fig. S2.

Since for the other two field directions [panels (b) and (c)] we find hysteric behavior we consider the kink/peak

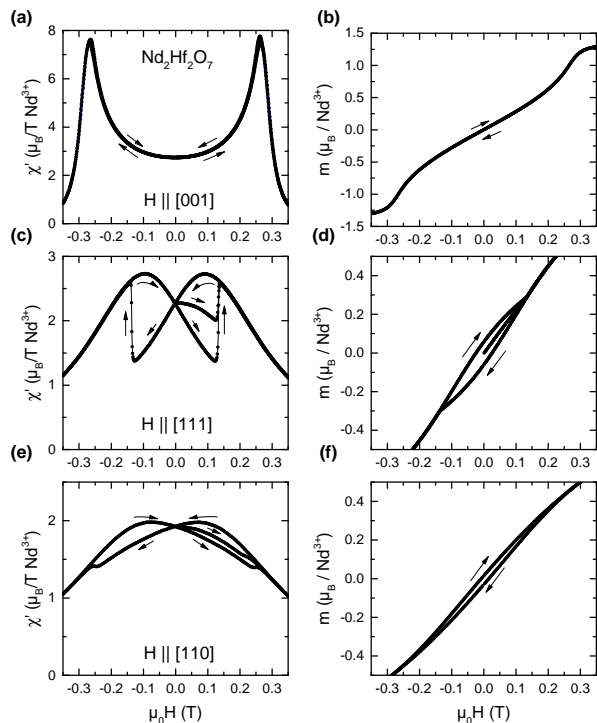


FIG. S6. Magnetic field dependency of the dynamic susceptibility (left panels) and magnetization (right panels) for  $H \parallel [001]$  (a,b),  $H \parallel [111]$  (c,d) and  $H \parallel [110]$  (e,f), obtained by integration, at a temperature of 0.12 K, 0.15 K and 0.11 K.

in  $\chi'(T)$  [Fig. 3(a) and Fig. S5] to signal the transition into the paramagnet. The transition line between the mixed and polarised domain phase was constructed by determining the temperature at each field below which the AC susceptibility shows a difference for different preparation fields [Fig. 3(a) and Fig. S5] and the end points of the hysteresis in the dynamic susceptibility.

We note that the phase boundary of the all-in-all-out order agrees quite well between  $H \parallel [001]$  and  $H \parallel [111]$ , but differs strongly in the case of  $H \parallel [110]$  in stark contrast to the results found in  $\text{Nd}_2\text{Zr}_2\text{O}_7$  [2].

### Domain walls in the all-in-all-out phase

In the main text we explain the observed anisotropic and inverted hysteresis and the negative remanent magnetization via the preferential formation of domains with boundaries which are polarised opposite to the applied magnetic field. This model explains (a) the negative remanence, (b) the heat pulse “effect”, (c) the mixing of states/partial preparation and (d) the anisotropy.

Here we provide additional details on the model underlying the all-in-all-out phase, the different realizations of the all-in-all-out state, the resulting domains, specifically the energetics/energy barriers favoring negatively polarised domain walls, and propose a simple free energy

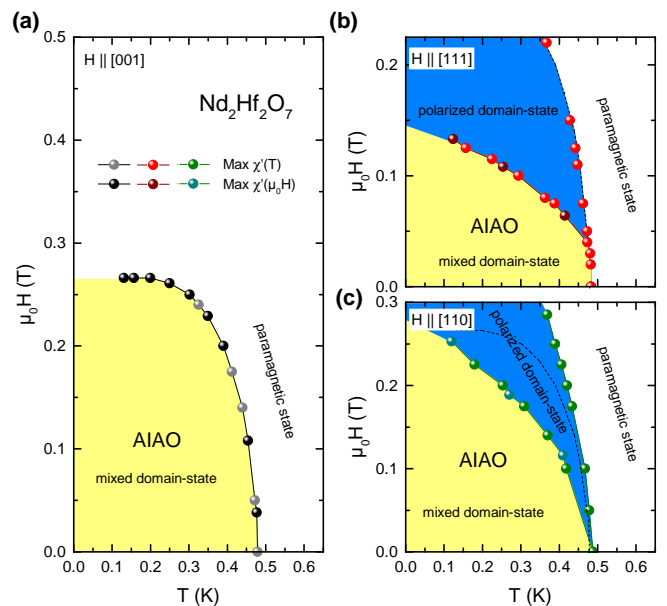


FIG. S7. Comparison of the phase diagrams of  $\text{Nd}_2\text{Hf}_2\text{O}_7$  for different field directions,  $H \parallel [001]$  (a),  $H \parallel [111]$  (b) [same as main text Fig. 3(b)], and  $H \parallel [110]$  (c). (a) The phase boundary of the all-in-all-out order was determined by the maximum in the temperature (grey) and field (black) dependence of the dynamic susceptibility. (b,c) The phase boundary of the all-in-all-out order was determined by the kinks/peaks of  $\chi'(T)$  (red/green spheres). The border between the mixed domain phase and the polarised domain phase was constructed by taking the temperature at each field (red/green spheres) below which the AC susceptibility starts to differ when polarising in negative compared to positive external fields  $|H| > H_c$  and the field strength of the end points of the hysteresis in the dynamic susceptibility (brown/grey spheres). The dashed black line in (b,c) is the phase boundary of the all-in-all-out order determined for  $H \parallel [001]$  in (a).

capturing the magnetization hysteresis.

### All-in-all-out order

Within the all-in-all-out order the spins on each sublattice point along their corresponding Ising anisotropy axis, i.e. one of the symmetry-equivalent  $\langle 111 \rangle$  directions, with all spins belonging to a given tetrahedron either pointing in towards or out from the center of the tetrahedron. Thus, the all-in-all-out order can be realized by two configurations, obtained from each other by flipping all spins on their Ising axis. Selecting the  $[111]$  axis, in these two realizations a fourth of the spins are oriented either parallel (AIAO) or antiparallel (AOAI) to the  $[111]$  axis.

### Energetics of the bulk phases in a field

Whereas for Ising spins both realizations of the all-in-all-out order are equivalent, which also remains true generally in absence of a magnetic field, this is not the case in finite field. An effective canting of the spins out of their local anisotropy axis, as a result of the dipolar-octupolar nature of the  $\text{Nd}^{3+}$  ions, leads to a gain of Zeeman energy which can differ between the configurations depending on the orientation of the magnetic field. Specifically, the states split for  $H \parallel [111]$ , but remain degenerate for  $H \parallel [001]$  [10].

This can be seen considering the general model for  $\text{Nd}^{3+}$  ions on the pyrochlore lattice [18]

$$H = \sum_{ij} J_z S_i^z S_j^z + J_x S_i^x S_j^x + J_{xz} S_i^x S_j^z + \sum_i g_{zz} \mathbf{B} \cdot \mathbf{e}_i^z S_i^z \quad (\text{S2})$$

written with respect to the local basis. The  $J_{xz}$  term can be removed by tilting the spins in the local  $x-z$  basis, thus, in the ground state configuration the spins do not point along the local  $z$ -axis anymore. In the new basis the model is characterised by the new couplings  $\tilde{J}_x$ ,  $\tilde{J}_z$  and the angle  $2\theta = \arctan(\frac{2J_{xz}}{J_x - J_z})$ .

We treat this microscopic hamiltonian classically and minimise the energy obtaining the magnetic field dependence of the energy and magnetisation of the AIAO and AOAI states.

For the related compound  $\text{Nd}_2\text{Zr}_2\text{O}_7$  this model has been shown to give quantitative agreement with the experimental neutron scattering results [19]. Since we do not have neutron scattering data we are not able to directly extract the coupling parameters. Instead we take the parameters obtained for  $\text{Nd}_2\text{Zr}_2\text{O}_7$  [19] as a starting point, noticing that there is some debate about the exact parameters [19, 20].

For  $\text{Nd}_2\text{Hf}_2\text{O}_7$  we assume an effective moment of the  $\text{Nd}^{3+}$  spins of  $\mu_{\text{eff}} = 2.32\mu_B$  related to  $g_{zz} = 2\mu_{\text{eff}}$ . To obtain an estimate of the other couplings, we compare the resulting magnetisation curves with the experimental data for  $H \parallel [100]$ . Reasonable agreement is achieved for  $J_x = 2.6 \times 0.103 \text{ meV}$ ,  $\tilde{J}_y = 0 \text{ meV}$ ,  $\tilde{J}_z = -2.6 \times 0.047 \text{ meV}$ , i.e. we rescale the couplings obtained for  $\text{Nd}_2\text{Zr}_2\text{O}_7$  of Ref. [19] by a factor of 2.6, and  $\theta = \pi/4$ .

Using these parameters we then consider the magnetic field dependence for fields oriented along  $[111]$  where the experimental data shows hysteresis. In Fig. S8 we clearly observe an energy splitting (panel a) of the two realisations of the all-in-all-out order and a different polarisability (panel b) due to spin canting of the AIAO and AOAI state.

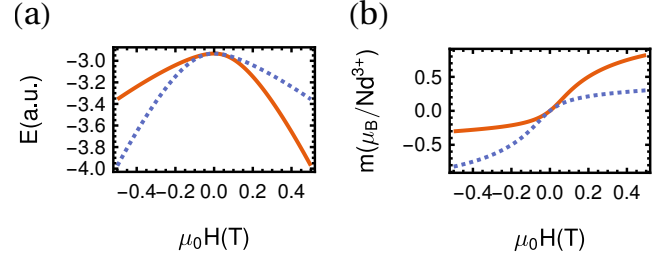


FIG. S8. Magnetic field dependence of the two realisations of the all-in-all-out order. (a) Energy  $E$  and (b) magnetisation  $m$  of the AIAO (solid lines) and AOAI (dashed lines) state for the magnetic field  $H$  oriented along  $[111]$ .

### Structure of spherical domain walls

The smallest closed spherical domain consists of 14 tetrahedra of AIAO (AOAI) in a background of AOAI (AIAO). These are oriented along one of the equivalent  $\langle 111 \rangle$  directions, with a ring of 6 tetrahedra shrinking to 3 and then 1 tetrahedron moving along the symmetry axis as depicted in Fig. S9 and Fig. S10 for a domain with symmetry axis  $[111]$ . The panels in Fig. S9 show the cor-

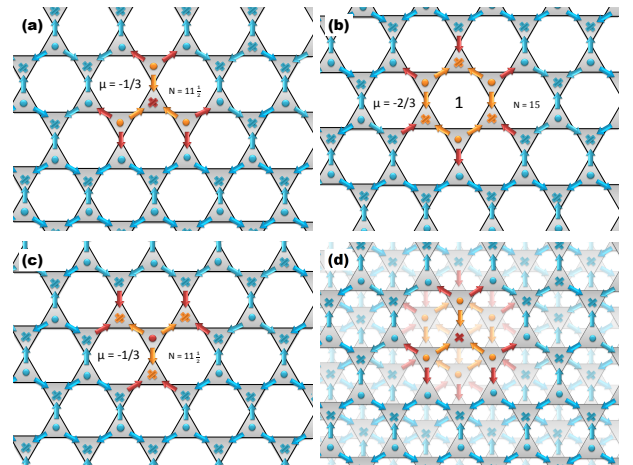


FIG. S9. Spherical domain with 3-In-1-Out boundaries oriented along  $[111]$ , resulting in a negative magnetization in  $[111]$  direction. View onto the kagome layer of the pyrochlore lattice perpendicular to  $[1\bar{1}0]$ . (x - spin pointing in,  $\bullet$  - spin pointing out). (a-c) view of different layers along  $[111]$ , (d) full view

responding view of the Kagome-layers of the pyrochlore lattice perpendicular to  $[1\bar{1}0]$ . The symmetry equivalent spherical domains are constructed the same way by orienting them along one of the four equivalent  $\langle 111 \rangle$  axes. Fig. S10 shows a 3D view of the same domain.

The depicted domain has 6 boundary tetrahedra with a moment of  $2\mu_{\text{eff}}$  in  $[\bar{1}11]$ , 6 with  $2\mu_{\text{eff}}$  in  $[1\bar{1}1]$ , 6 with  $2\mu_{\text{eff}}$  in  $[11\bar{1}]$  and 2 with  $2\mu_{\text{eff}}$  in  $[111]$  which results in a total magnetic moment of  $-4\mu_{\text{eff}}$  in  $[111]$ , and equivalently for the other symmetry related domains. We em-

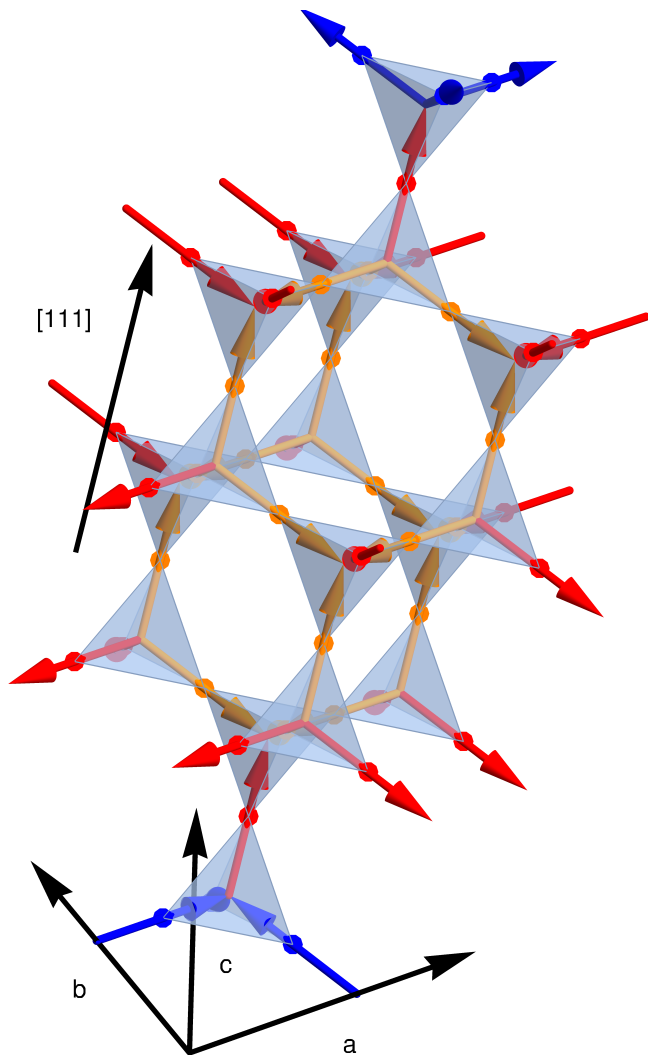


FIG. S10. 3D view of spherical domain with 3-In-1-Out boundaries oriented along  $[111]$ , resulting in a negative magnetization in  $[111]$  direction. Blue (orange) spins belong to AOAI (AIAO) bulk tetrahedra, red spins are boundary spins of the AIAO domain.

phasise that the total magnetic moment of an equal number of all possible domains vanishes.

Using the microscopic hamiltonian (Eq. S2) with the parameters as discussed above we can estimate the energy cost and magnetisation per tetrahedron of these domains as  $E_{\text{DW}} \approx 2 \text{ meV}$  and  $m_{\text{DW}} \approx 0.3 \mu_B$ .

#### Energy barriers to domain wall growth

Whereas in zero field all domains and the corresponding intermediate stages of their growth have the same energy, in a finite field oriented along one of the symmetry axes, e.g.  $[111]$ , this is no longer the case. Note that for a field applied along  $[001]$ , the magnetic moments of the different spherical domains projected onto the field

direction is the same, and no specific domain is favored.

To illustrate that the formation of negatively polarised spherical domains is favoured in positive field we consider the specific case of a magnetic field oriented along  $[111]$  and the domain in Fig. S9 and Fig. S10. Considering the growth process along the  $[111]$  axis we have the following stages: A single domain tetrahedra with a vanishing moment, 4 flipped domain tetrahedra with a total moment of  $2 \mu_{\text{eff}}$ , 10 domain tetrahedra with a moment of  $0 \mu_{\text{eff}}$ , 13 domain tetrahedra with a moment of  $-6 \mu_{\text{eff}}$  and finally the close spherical domain with 14 domain tetrahedra and a moment of  $-4 \mu_{\text{eff}}$ . We surprisingly observe that the first stages of domain growth have the opposite magnetisation compared to the final closed domain. The same is true for the alternative growth path, starting with the ring of 6 tetrahedra with a moment of  $4 \mu_{\text{eff}}$ , adding each 3 tetrahedra above and below for a moment of  $-8 \mu_{\text{eff}}$  and ending with the closed spherical domain with  $-4 \mu_{\text{eff}}$ .

Thus, in a positive field along  $[111]$  the formation of the intermediate stages of this type of domain is favoured compared to the ones oriented along the other symmetry axes.

#### Free energy

Based on the observations made above, we propose a simple model free energy to capture the inverted hysteresis. As the main non-equilibrium ingredient we assume that in a preformed fully polarised phase of either AIAO or AOAI the domain walls form predominantly with a magnetization opposite to the magnetic field, due to energy barriers discussed above.

The free energy is constructed in the following way: The existence of domains is due to the gain in entropy compared to a pure single domain state, and as the most basic approximation we simply take the random mixing entropy

$$S = x \ln(x) + (1 - x) \ln(1 - x), \quad (\text{S3})$$

where  $x$  is the volume fraction of one of the bulk phases.

Since in a finite field the AIAO/AOAI domains have different energies, we also include an energy term for the bulk phases

$$\begin{aligned} E_{\text{Bulk}} &= x E_{\text{AIAO}}(H) + (1 - x) E_{\text{AOAI}}(H) \\ &= x [E_{\text{AIAO}}(H) - E_{\text{AOAI}}(H)] + \text{const.} \end{aligned} \quad (\text{S4})$$

where we obtain the different field dependent energies for the two realisations of the all-in-all-out order from a classical treatment of the microscopic Hamiltonian S2.

In addition, the domain walls between the bulk phases contribute to the energy. The surface in random mixing is proportional to  $x(1-x)$  which results in an energy cost

$$E_S = x(1-x) [E_{\text{DW}} - m_{\text{DW}} H], \quad (\text{S5})$$

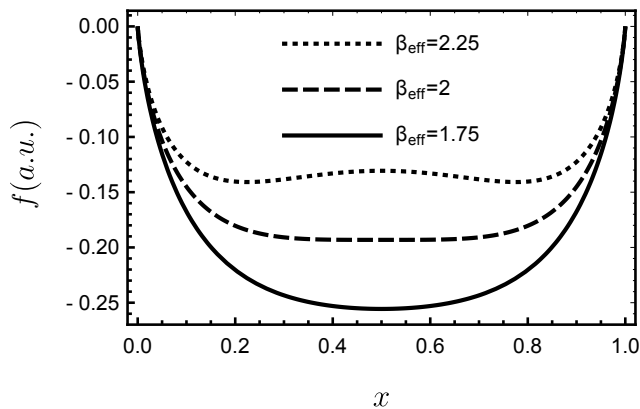


FIG. S11. Phase transition occurring in the model free energy. The free energy  $F$  shows qualitatively different behavior as a function of the bulk phase volume fractions  $x$  when changing the parameters  $\beta_{\text{eff}} = (\beta + m_{\text{DW}}H)/T$ , here shown for  $\alpha = 0$ . Below  $\beta_{\text{eff}} = 2$  we obtain a unique equal-density mixture phase, whereas above there are two high-low density mixture phases.

with a constant contribution  $E_{\text{DW}}$  due to broken bonds at the domain boundary and a Zeeman energy due to the domain wall magnetization  $m_{\text{DW}}$ .

The domain wall surface magnetization,  $m_{\text{DW}}$ , is the crucial non-equilibrium input, we take it to be opposite to the magnetic field direction due to the energy barriers to domain wall growth which favor this type of domains. Moreover, it depends on the initially prepared state: it takes its maximal value for the fully polarised initial condition, and decreases down to zero for the unpolarised condition.

In total we model the free energy for a mixture of AIAO and AOAI domains with domain walls as

$$f = x [E_{\text{AIAO}}(H) - E_{\text{AOAI}}(H)] + x(1-x) [E_{\text{DW}} - m_{\text{DW}}H] + T [x \ln(x) + (1-x) \ln(1-x)] \quad (\text{S6})$$

Let's first discuss the case of balanced bulk phases, e.g. no spin canting, hence, no energy difference between the bulk states ( $E_{\text{AIAO}} = E_{\text{AOAI}}$ ). In that case we obtain a phase-transition as a function of  $\beta_{\text{eff}} = (E_{\text{DW}} - m_{\text{DW}}H)/T$  between a unique equal mixture with  $x = 0.5$  for  $\beta_{\text{eff}} < 2$ , and a high/low density phase with  $x \neq 0.5$  and two solutions for  $\beta_{\text{eff}} > 2$  as shown in Fig. S11.

Considering imbalanced bulk states, e.g. assuming a cubic energy difference ( $E_{\text{AIAO}} - E_{\text{AOAI}} = \alpha H^3$ ), one of the solutions becomes meta-stable up to a critical field strength where a transition into a unique high/low density-phase occurs.

This simple model naturally leads to an inverted hysteresis loop, Fig. S12. For the positively polarised initial condition ( $m_{\text{DW}} < 0$ , solid curve in Fig. S12(a)) the volume fraction evolves smoothly from  $x = 1$  at large positive field down to a critical negative field where the

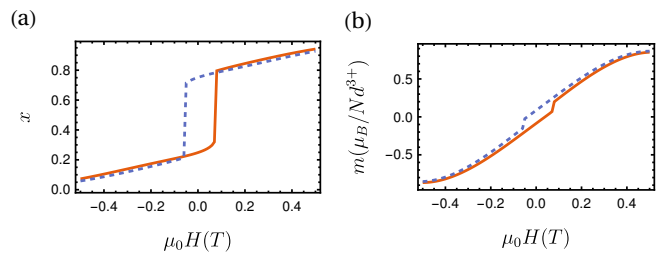


FIG. S12. Magnetic field dependence resulting from the model free energy for negatively (dashed) and positively (solid) polarised initial states ( $m_{\text{DW}} = \pm 2.1$ ). (a) Bulk phase volume fractions  $x$  and (b) magnetization  $m$  (including the bulk and domain wall contributions) as a function of magnetic field  $H$ .

phase becomes unstable and the volume fraction jumps, and then connects smoothly to the  $x = 0$  negatively polarised phase. Similarly, for the negatively polarised initial condition ( $m_{\text{DW}} > 0$ , dashed curve in Fig. S12(a)) the state evolves smoothly from  $x = 0$  at large negative fields up to a critical positive field where the volume fraction jumps, and then connects to the positively polarised state. Due to the domain wall magnetization the resulting magnetization curve shows an inverted hysteresis (Fig. S12(b)) with a remanence at  $H = 0$  which is negative (positive) for the positively (negatively) polarised initial states (solid/dashed curves respectively). We emphasise that this toy model demonstrates that the basic phenomenology described here does not depend on the specific choices made for the comparison with the experimental data detailed next.

Finally, we turn to the comparison with the experiment. We obtain the energy (and magnetisation dependence) of the bulk phases  $E_{\text{AIAO/AOAI}}(H)$  from a classical treatment of the microscopic Hamiltonian as described above. Based on the discussed spherical domain structure and the microscopic hamiltonian we obtain  $E_{\text{DW}} = 2.3 \text{ meV}$  and  $m_{\text{DW}} = \pm 0.3 \mu_B$  (see above). The absolute temperature, and hence the absolute energy scale, remains a free parameter since the entropy of the resulting mixture is only roughly approximated by the random mixing entropy and would depend on the specific configuration, sizes and forms of the domains.

Using above parameters in the model free energy (Eq. S6) we obtain the hysteresis behavior shown in Fig. S13 and in the main text.

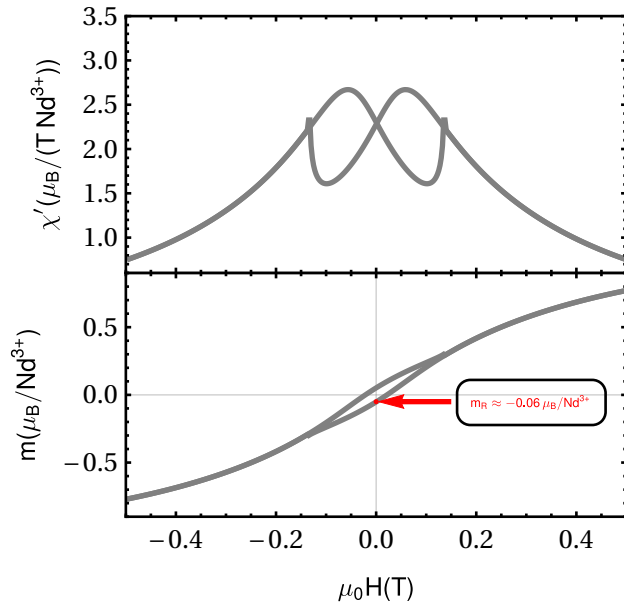


FIG. S13. Theoretical magnetic-field dependence of (a) the susceptibility and (b) the magnetisation. Results obtained from the proposed model free energy using the energy and magnetisation curves of the AIAO and AOAI states obtained from the classical treatment of the microscopic hamiltonian.